Chemical Science

ROYAL SOCIETY OF CHEMISTRY

EDGE ARTICLE

View Article Online
View Journal | View Issue

Cite this: *Chem. Sci.*, 2025, **16**, 784

All publication charges for this article have been paid for by the Royal Society of Chemistry

Received 11th July 2024
Accepted 6th November 2024

DOI: 10.1039/d4sc04607b

rsc.li/chemical-science

Ag(I) emitters with ultrafast spin-flip dynamics for high-efficiency electroluminescence†

Ao Ying,‡[a] Nengquan Li, ‡[b] Xingyu Chen,[c] Jianlong Xia, [c] Chuluo Yang *[b] and Shaolong Gong *[a]

Carbene-metal-amide (CMA) complexes are appealing emitters for organic light-emitting diodes (OLEDs). However, little is known about silver(I)-CMA complexes, particularly electroluminescent ones. Here we report a series of Ag(I)-CMA complexes prepared using benzothiophene-fused carbazole derivatives as amide ligands. These complexes emit *via* thermally activated delayed fluorescence (TADF), together with high photoluminescence quantum yields of up to 72% in thin films. By strengthening the π-donating ability of the amide ligands, ultrashort emission lifetimes of down to 144 ns in thin films and 11 ns in solution (with a radiative rate constant of $\sim 10^7$ s^{-1}) are realized, among the shortest lifetimes for TADF emitters. Key to this unique feature is the ultrafast spin-flip dynamics consisting of forward and reverse intersystem crossing rates of up to $\sim 10^9$ s^{-1} and $\sim 10^8$ s^{-1}, respectively, verified by the transient absorption spectroscopic study. The resulting solution-processed OLEDs based on the optimal complex afford record external quantum efficiencies of 16.2% at maximum and 13.4% at 1000 nits, representing the state-of-the-art performance for Ag(I) emitters. This work presents an effective approach for the development of short-lived TADF materials for high-efficiency OLEDs.

Introduction

In comparison with well-established iridium(III) and platinum(II) phosphors, luminescent coinage metal(I) complexes, particularly copper(I) and silver(I) complexes, have been studied for decades as promising cost-effective alternatives for applications in photocatalysis and optoelectronics.[1–3] Phosphorescence from metal-to-ligand charge transfer (MLCT) excited states is the main focus for coinage metal(I) emitters at the early stage.[4,5] However, with respect to Ir(III) and Pt(II) complexes, Cu(I) and Ag(I) complexes usually show inefficient phosphorescence because of their slower intersystem crossing (ISC) rates from S_1 to T_1 and from T_1 to S_0, originating from moderate spin–orbital coupling (SOC) parameters of the Cu (857 cm^{-1}) and Ag (1830 cm^{-1}) nuclei.[6,7] In the past decade, thermally activated delayed fluorescence (TADF) has been demonstrated in numerous Cu(I) complexes by introducing MLCT, halogen-to-ligand charge transfer (XLCT) and/or ligand-to-ligand charge transfer (LLCT) into excited states.[8–14] Compared with Cu(I) complexes, Ag(I) complexes are more appealing candidates for short-lived TADF emitters due to the larger atomic number of the silver atom according to semi-classical Marcus theory.[15] Despite the fact that some Ag(I) complexes have been developed to exhibit temperature-dependent photophysical behaviors,[16] the first TADF Ag(I) complex was reported by Osawa and co-workers only in 2013 (Fig. 1a).[17] The TADF Ag(I) complexes are still scarce. The main limitations are the considerably high oxidation potential and low-lying d-orbitals of the Ag(I) center, preventing the participation of d electrons of the Ag atom in frontier occupied orbitals.[18–23] As a result, the excited states of the Ag(I) complexes often feature a ligand-centered nature, leading to long-lived phosphorescence together with low radiative rates (k_r).[13,14,24–26] To access the TADF channel of Ag(I) emitters, one of the mainstream approaches is to use strongly electron-donating ligands such as phosphines, which can destabilize the d-orbital of the central Ag atom and thus allow for metal-involved charge transfer in excited states.[18–24,27–29] For instance, Yersin and co-workers developed a series of four-coordinate Ag(I) complexes using phosphine and phenanthroline derivatives as ligands (Fig. 1a).[19,21,23–25,27,29] With the introduction of carborane subunits, the phosphine ligands have strong donor strength and thus render efficient TADF from excited states featuring MLCT and LLCT.[19,29] Similarly, Lu *et al.* constructed a series of TADF Ag(I) complexes (Fig. 1a) bearing

[a]*College of Chemistry and Molecular Sciences, Hubei Key Laboratory on Organic and Polymeric Optoelectronic Materials, Wuhan University, Wuhan 430072, China. E-mail: slgong@whu.edu.cn*

[b]*Shenzhen Key Laboratory of New Display and Storage Materials, College of Materials Science and Engineering, Shenzhen University, Shenzhen 518060, China. E-mail: clyang@szu.edu.cn*

[c]*State Key Laboratory of Advanced Technology for Materials Synthesis and Processing, Center of Smart Materials and Devices, International School of Materials Science and Engineering, Wuhan University of Technology, Wuhan 430070, China*

† Electronic supplementary information (ESI) available. See DOI: https://doi.org/10.1039/d4sc04607b

‡ These authors contributed equally to this work.

P^P and N^N ligands in a donor–acceptor motif.[30] The resulting complexes feature LLCT nature with less metal contribution (<20%) in excited states. Despite the above promising results, the emission lifetimes of these Ag(I) complexes are still on the μs-scale (>1 μs) and are comparable with conventional TADF or phosphorescent emitters.[31–34] How to further accelerate the spin-flip process of Ag(I) complexes is still a formidable challenge. In addition, only two electroluminescent mononuclear Ag(I) emitters have been reported so far, yet with external quantum efficiencies (EQEs) of <15%.[35,36] This device performance is far away from the theoretical limit of 20–30% EQEs for organic light-emitting diodes (OLEDs).[37] In this regard, the search for high-performance Ag(I) complexes is of vital importance for both fundamental investigation and practical applications.

Recently, paramount attention has been paid to a new category of coinage metal(I) complexes bearing a carbene-metal-amide (CMA) motif, due to their distinct TADF properties and high emission performance.[7,38] In these complexes, the central metal serves as an electronic bridge to facilitate the long-range p-orbital coupling between the carbene and amide ligands, with limited metal contribution (<15%) to this CT process.[39] As a result, CMA complexes have a unique metal-perturbed LLCT nature in excited states, giving rise to distinct TADF properties and fast radiative rates. Despite the small metal contribution to excited states of CMA complexes, the introduction of the metal linkage can still enhance the SOC, accelerate the spin-flip dynamics and thus shorten the exciton lifetimes.[38h–j,39,40] Therefore, CMA complexes are ideal candidates for the development of short-lived TADF emitters. In the past few years, the development of CMA complexes has mainly focused on Cu(I) and Au(I) complexes, and some of them have achieved comparable emission performance to Ir(III) and Pt(II) complexes.[39] In contrast to MLCT-featured phosphorescent complexes, the emission lifetimes of CMA complexes are mainly governed by the singlet–triplet energy difference (ΔE_{ST}), rather than the SOC of the central metals.[38l,n] In general, Ag(I)-CMA complexes exhibit shortened emission lifetimes compared with Cu(I) and Au(I) analogues, due to reduced ΔE_{ST} originating from the prolonged metal–ligand bond lengths.[38e,i] This feature makes Ag(I)-CMA complexes appealing emitters for OLEDs with low efficiency roll-off. However, there are only a few reports on Ag(I)-CMA complexes. Only one example of OLEDs based on Ag(I)-CMA complexes was demonstrated by Romanov *et al.* (Fig. 1)[35] but with moderate EQEs of 13.7% and 11.0% in vacuum- and solution-processed devices, respectively. This proof-of-concept application in OLEDs pinpoints the large potential of Ag(I)-CMA emitters.

Ligand engineering is the most popular way of modulating the optoelectronic properties of CMA complexes. We recently demonstrated that chalcogen-heterocyclic engineering on the amide ligand can optimize the conformation and the related optical properties of Cu(I)-CMA complexes, giving rise to a record EQE of 28.6% for Cu(I)-OLEDs.[41] Following this revelation, we herein developed a series of Ag(I)-CMA complexes, Ag-12BT-CN, Ag-12BT, and Ag-12BT-OMe, using benzothiophene-

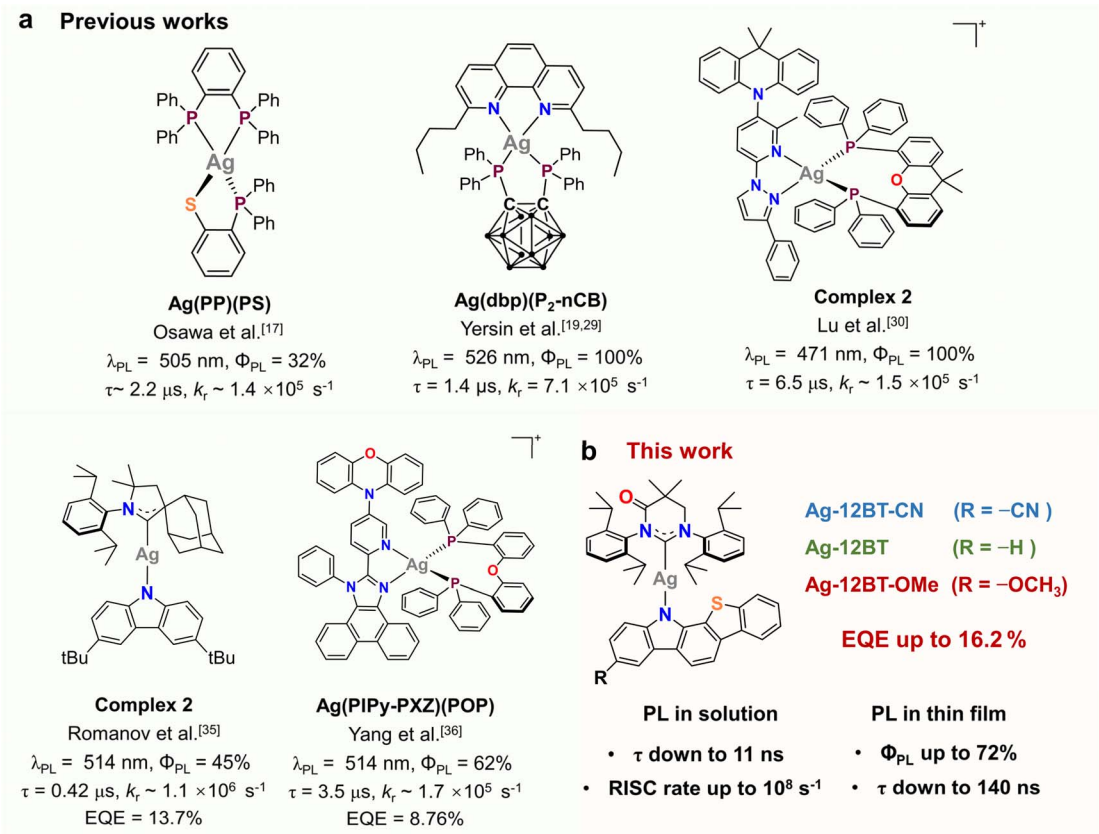

Fig. 1 (a) Selected examples of TADF Ag(I) complexes reported in the literature. (b) Chemical structures of the Ag(I)-CMA complexes in this work.

fused carbazole derivatives, 12*H*-benzo[4,5]thieno[2,3-*a*]carbazole-3-carbonitrile (12BT-CN), 12*H*-benzo[4,5]thieno[2,3-*a*]carbazole (12BT), and 3-methoxy-12*H*-benzo[4,5]thieno[2,3-*a*]carbazole (12BT-OMe), as amide ligands to combine with a widely used carbene ligand of MAC* (Fig. 1b). With the fusion of a benzothiophene subunit, Ag-12BT-OMe demonstrated a distinct secondary metal–ligand interaction between the Ag center and amide ligand, as verified by theoretical simulation and single-crystal structure analysis. These complexes exhibited distinct TADF nature with high photoluminescence quantum yields (Φ_{PL}) of up to 72% and k_r of up to 2.2×10^6 s^{-1} in thin films. Intriguingly, Ag-12BT and Ag-12BT-OMe delivered ultrashort emission lifetimes of 70 and 11 ns in solution, respectively, representing the shortest lifetime for TADF emitters. This unique feature is strongly associated with ultrafast spin-flip dynamics consisting of ultrahigh rate constants of $\sim 10^9$ s^{-1} and $\sim 10^8$ s^{-1} for the forward and reverse intersystem crossing (ISC) between T_1 and S_1, respectively, as verified by the transient absorption spectroscopic study. The solution-processed OLEDs based on the optimal emitter Ag(I)-12BT realized outstanding EL performance with record EQEs of 16.2% and 13.4% at maximum and 1000 cd m^{-2}, respectively.

Results and discussion

Before synthesis, theoretical calculations were conducted on these Ag(I) complexes to study their electronic structures and excited states. As shown in Fig. S1,† all the Ag(I) complexes exhibited nearly coplanar conformations with small ligand–ligand dihedral angles of 10° to 12°, along with nearly linear ∠C–Ag–N angles of 173° to 175°. Meanwhile, these complexes possessed C–Ag and Ag–N bond lengths of ~2.1 Å, similar to the values reported in the literature.[38l] In comparison with their Cu(I) and Au(I) analogues, the Ag(I) complexes possess prolonged $C_{carbene}\cdots N_{carbazole}$ distances, resulting in more separated hole–electron distributions and longer-range LLCT (Fig. 2). For Ag-12BT-CN and Ag-12BT, the center of the hole in their S_1 excited states mainly lied near the $N_{carbazole}$ atom, whereas the $-OCH_3$ group of Ag-12BT-OMe dispersed the positive charge and thus shifted the hole center away from the $N_{carbazole}$ atom. Therefore, Ag-12BT-OMe had the longest hole–electron distance of 6.45 Å in its S_1 excited state. Moreover, all the complexes had dominant LLCT nature in both S_1 and T_1 excited states together with the *ca.* 2–4% contributions from the central silver (Fig. 2a and Table S1†), leading to a metal-perturbed intraligand charge-transfer feature. Meanwhile, the small transition contributions from the metal center also prevented the Renner–Teller distortion and direct phosphorescence, supported by the CT-featured emission profiles at 300 and 77 K (Fig. S2†). Furthermore, the introduction of the –CN/–OCH_3 group can finely modulate the π-donating ability of the amide ligands and thus render HOMO levels of the complexes tunable (Fig. S3†). Therefore, the S_1 levels of the Ag(I) complexes follow the order of 2.47 eV (Ag-12BT-CN, 502 nm) > 2.22 eV (Ag-

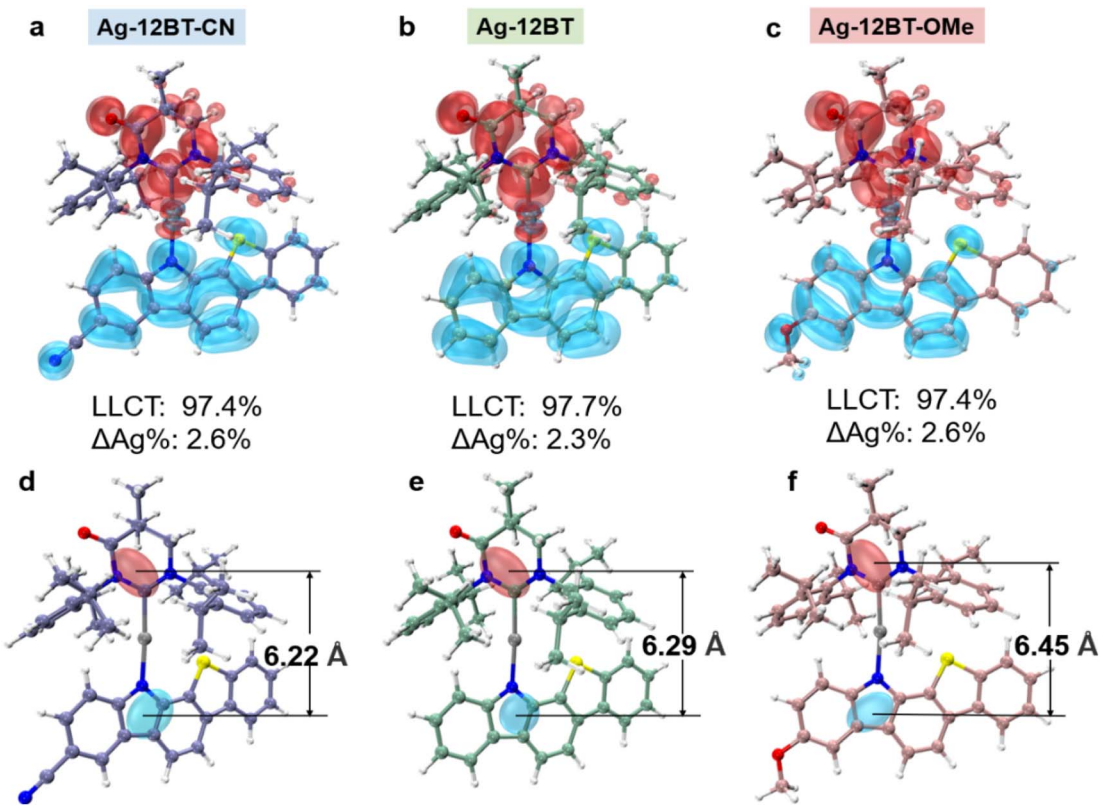

Fig. 2 The hole–electron distribution of S_1 excited states for (a) Ag-12BT-CN, (b) Ag-12BT, and (c) Ag-12BT-OMe. ΔAg represents the difference in metal participation before and after excitation. The centroid distance between holes and electrons of (d) Ag-12BT-CN, (e) Ag-12BT, and (f) Ag-12BT-OMe. The distributions and centroids of holes and electrons are colored blue and red, respectively.

12BT, 558 nm) > 2.02 eV (Ag-12BT-OMe, 614 nm), depending on the π-donating strength of the amide ligands. Meanwhile, with respect to Ag-12BT-CN and Ag-12BT, Ag-12BT-OMe delivered the smallest ΔE_{ST} of 0.05 eV (Fig. S3†), which stemmed from the prolonged hole–electron distance. Thanks to the large steric hindrance between the carbene and benzothiophene subunits, these complexes have slightly twisted S_1 conformations with lower energies compared with the orthogonal conformers (Fig. S4 and S5†), different from the orthogonal S_1 conformation in most CMA complexes. Furthermore, the root mean square deviation (RMSD) between S_0 and S_1 in these complexes follows the trend of 0.29 Å (Ag-12BT-CN) ≈ 0.22 Å (Ag-12BT-CN) < 0.78 Å (Ag-12BT-OMe), suggesting that Ag-12BT-CN and Ag-12BT have limited structure reorganization and could be better emitters (Fig. S6†).

The key intermediate (MAC)AgCl was prepared according to the procedures reported in the literature.[38l] The amide ligands of 12BT-CN and 12BT-OMe were synthesized *via* a two-step route including Pd-catalyzed C–N coupling and Pd-catalyzed intramolecular cyclization reactions (Scheme S1†). The target Ag(I) complexes were obtained by a nucleophilic reaction between the key intermediate of (MAC)AgCl and the respective amide ligands. $^1H/^{13}C$ nuclear magnetic resonance and ^1H–^1H COSY spectroscopy, high-resolution mass spectroscopy and elemental analysis were conducted to characterize chemical structures of the Ag(I) complexes. Furthermore, the single crystal of Ag-12BT-OMe was obtained by layering of CH_2Cl_2 solution with *n*-hexane. As depicted in Fig. S7 and Tables S2, S3,† Ag-12BT-OMe exhibited similar C–Ag and Ag–N bond lengths of 2.103(5) and 2.082(4) Å, respectively, together with a small ligand–ligand dihedral angle of ∼14.3° and a nearly linear ∠C–Ag–N angle of 171.85(17)°.[42] These structure features are basically consistent with the theoretical results. Furthermore, Ag-12BT-OMe delivered the Ag···S distance of 3.44 Å, smaller than the sum of van der Waals radii of the Ag and S atoms (3.52 Å).[43] This pinpoints the existence of secondary metal–ligand interactions between the Ag atom and amide ligand in Ag-12BT-OMe. Atom in molecular (AIM) and natural bonding orbital (NBO) calculations further verified that the nature of such secondary metal–ligand interactions is attractive noncovalent interactions between the n orbital of the sulfur atom and the s orbital of the silver nucleus (Fig. S8†).[44] Such interactions can stabilize the flattened conformations of these complexes to some extent and thus can be favorable to maintain high oscillator strength and suppress excited state reorganization.[41]

All the complexes underwent amide-ligand attributed irreversible oxidation processes (Fig. S9†). According to the half-wave potentials (calibrated *versus* ferrocenium/ferrocene), the HOMO levels of these complexes gradually increased in the order of −5.64 eV (Ag-12BT-CN) < −5.44 eV (Ag-12BT) < −5.27 eV (Ag-12BT-OMe), in accordance with the simulated results. Combined with the optical bandgaps, the LUMO levels of these complexes were estimated to be from −2.84 to −2.86 eV.

As pictured in Fig. 3a, despite the similar ligand-contributed absorption below 400 nm, the LLCT absorption peaks of these complexes were gradually red-shifted, following the trend of 405 nm (Ag-12BT-CN) < 424 nm (Ag-12BT) < 430 nm (Ag-12BT-OMe).

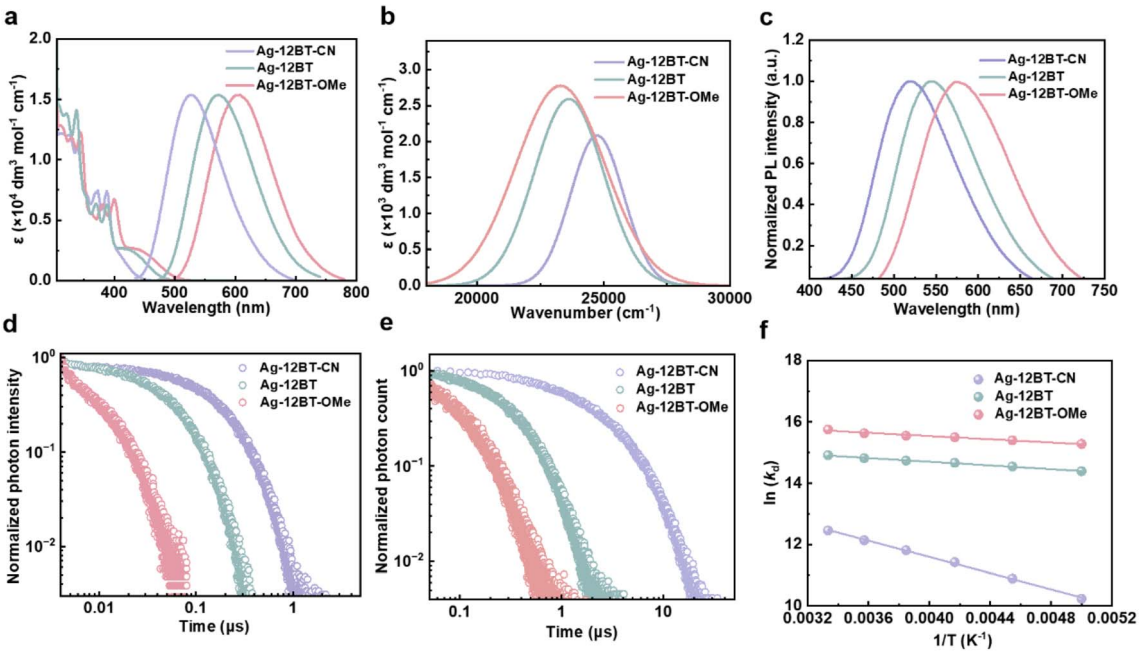

Fig. 3 (a) UV-vis absorption and normalized fluorescence spectra of Ag-12BT-CN, Ag-12BT, and Ag-12BT-OMe in toluene solutions (10^{-4} M, 300 K). (b) LLCT band of Ag-12BT-CN, Ag-12BT, and Ag-12BT-OMe in toluene solutions. The spectra were extracted by the Gaussian-type peak analysis. (c) Normalized fluorescence spectra of Ag-12BT-CN, Ag-12BT, and Ag-12BT-OMe in mCP-doped films with a 30 wt% doping concentration, following excitation at 350 nm. Transient PL decay curves of Ag-12BT-CN, Ag-12BT, and Ag-12BT-OMe (d) in toluene solutions (10^{-4} M, 300 K) and (e) mCP-doped films with a 30 wt% doping concentration, following excitation at 375 nm. (f) Arrhenius-type fit of the temperature-dependent lifetime data (symbols) to eqn S2† (line) for the doped films of Ag-12BT-CN, Ag-12BT, and Ag-12BT-OMe.

Table 1 Photophysical properties of these complexes in solution and film states

Complex	λ_{PL} [nm]	Φ_{PL} [%]	τ_d [μs]	k_r [10^6 s^{-1}]	k_{nr} [10^6 s^{-1}]	$\Delta E_{ST}{}^{a/b}$ [meV]
In toluene (10^{-4}M)						
Ag-12BT-CN	527	25	0.21	1.2	3.6	—
Ag-12BT	571	32	0.070	4.6	9.8	—
Ag-12BT-OMe	608	10	0.011	9.1	91	—
30 wt% mCP-doped film						
Ag-12BT-CN	521	60	3.9	0.2	0.1	96/80
Ag-12BT	545	72	0.33	2.2	0.9	24/33
Ag-12BT-OMe	571	23	0.14	1.6	6.7	22/28

[a] Fitted from the Boltzmann-type dynamic model. [b] Fitted from the Arrhenius-type dynamic model.

Moreover, their LLCT absorption bands had enhanced intensity and broadened width with the gradually increasing π-donating strength of the amide ligands (Fig. 3b). Accordingly, the experimental S_1–S_0 oscillator strength of these complexes was determined to be 0.022 for Ag-12BT-CN, 0.037 for Ag-12BT, and 0.049 for Ag-12BT-OMe. Similar to the sequence of the LLCT absorption bands, these complexes displayed tunable emission profiles spanning from 527 to 608 nm in solution and from 521 to 571 nm in thin films [30 wt% in mCP (*N*,*N*-dicarbazolyl-3,5-benzene)] (Table 1, Fig. 3a and c). To gain insight into the photophysical behaviors of these Ag(I) complexes, transient photoluminescence (PL) curves were obtained. Inspiringly, Ag-12BT and Ag-12BT-OMe delivered shorter emission lifetimes of 70 and 11 ns, respectively, compared with that of Ag-12BT-CN (210 ns). Under aerated conditions, the lifetimes of these complexes were significantly shortened, implying the participation of triplet excitons (Fig. S10†). Benefitting from the extremely short emission lifetime, Ag-12BT-OMe has a large k_r constant of 9.1×10^6 s^{-1}, among the best values for Ag(I) complexes.[16–25,35,38f,l] In the rigid mCP host matrix, the emission lifetimes of Ag-12BT and Ag-12BT-OMe were still as short as 330 and 144 ns, respectively, yet Ag-12BT-CN delivered a longer lifetime of 3.9 μs (Fig. 3e and Table 1). Moreover, Ag-12BT-CN and Ag-12BT delivered significantly higher Φ_{PL} of 60% and 72% compared with that of Ag-12BT-OMe (Φ_{PL} = 23%). This result matches well with the limited excited state reorganization of Ag-12BT-CN and Ag-12BT with respect to Ag-12BT-OMe in the above theoretical study, indicating that the Φ_{PL} of these Ag(I) complexes are mainly influenced by nonradiative processes rather than their radiative probabilities (related to oscillator strength). In this context, Ag-12BT demonstrated the highest k_r of 2.2×10^6 s^{-1} in the film state. Temperature-dependent lifetimes of these complexes were conducted to determine their emission origins. As illustrated in Fig. S11 and S12,† when cooled down to 77 K, all the complexes delivered nearly one order of magnitude longer average decay lifetimes than those at 300 K (Table S4†), establishing the TADF nature of these Ag(I) complexes. Moreover, the local triplet excited states (^{3}LE) of the amide ligands are energetically higher than the CT-featured S_1 states of the corresponding complexes, preventing the direct phosphorescence from the amide ligands (Fig. S2†). Subsequently, the ΔE_{ST} of these complexes was determined to be 96/80 meV for Ag-12BT-CN, 24/33 meV for Ag-12BT, and 22/28 meV for Ag-12BT-OMe, according to the Boltzmann- and Arrhenius-type fittings (Fig. 3f and S12†). In this regard, the smallest ΔE_{ST} is one of the main reasons for the shortest TADF lifetime of Ag-12BT-OMe, which originated from the longer-range LLCT (Fig. 2). To reveal the influence of the central Ag ions on the spin-flip processes between S_1 and T_1 states, the SOC constants between S_1 and T_1 were evaluated for these complexes. As listed in Table S1,† the SOC constants evolved in the order of 0.06 cm^{-1} (Ag-12BT-CN) < 1.53 cm^{-1} (Ag-12BT) < 1.60 cm^{-1} (Ag-12BT-OMe), basically opposite to the trend of TADF lifetimes. We also noted that this series of Ag(I) emitters exhibited smaller Φ_{PL} and shorter emission lifetimes with respect to their Cu(I) counterpart Cu-12BT in our previous work.[41] This phenomenon roots from the larger atomic radii of silver, which lead to longer metal–ligand bonds. On one hand, the longer C–Ag and Ag–N bonds enable more separated HOMO–LUMO distributions and smaller ΔE_{ST} values, thus rendering shorter emission lifetimes. On the other hand, the longer coordinate bonds reduce the steric hindrance between the carbene and amide ligands, allowing higher ligand–ligand rotation/twist freedom. This could result in higher nonradiative rates and lower Φ_{PL}. Considering that the singlet radiative rate ($k_{r,s}$) is another critical rate-determining step for the TADF process, we estimated $k_{r,s}$ based on a two-level Boltzmann dynamic model. As shown in Fig. S12,† Ag-12BT and Ag-12BT-OMe exhibited larger $k_{r,s}$ of 2.2×10^7 s^{-1} and 6.9×10^7 s^{-1} than Ag-12BT-CN ($k_{r,s} = 7.3 \times 10^6$ s^{-1}) in the film state, which originated from their larger S_1–S_0 oscillator strength according to the Einstein relations of radiative lifetime (Fig. 3b).[45] In this sense, the enhanced π-donating strength of the amide ligands not only reduces the ΔE_{ST} for these Ag(I) emitters but also accelerates the S_1–S_0 radiative rate *via* enhancing the oscillator strength.

To further picture the exciton dynamics of these complexes, fs- and ns-scale transient absorption (TA) spectroscopy studies were conducted in chlorobenzene solution (2 mg mL^{-1}). In the first 2 ps, the positive signals of photoinduced absorption (PIA) for all the complexes were significantly increased, which can be assigned to the formation of charge transfer S_1 excited states.

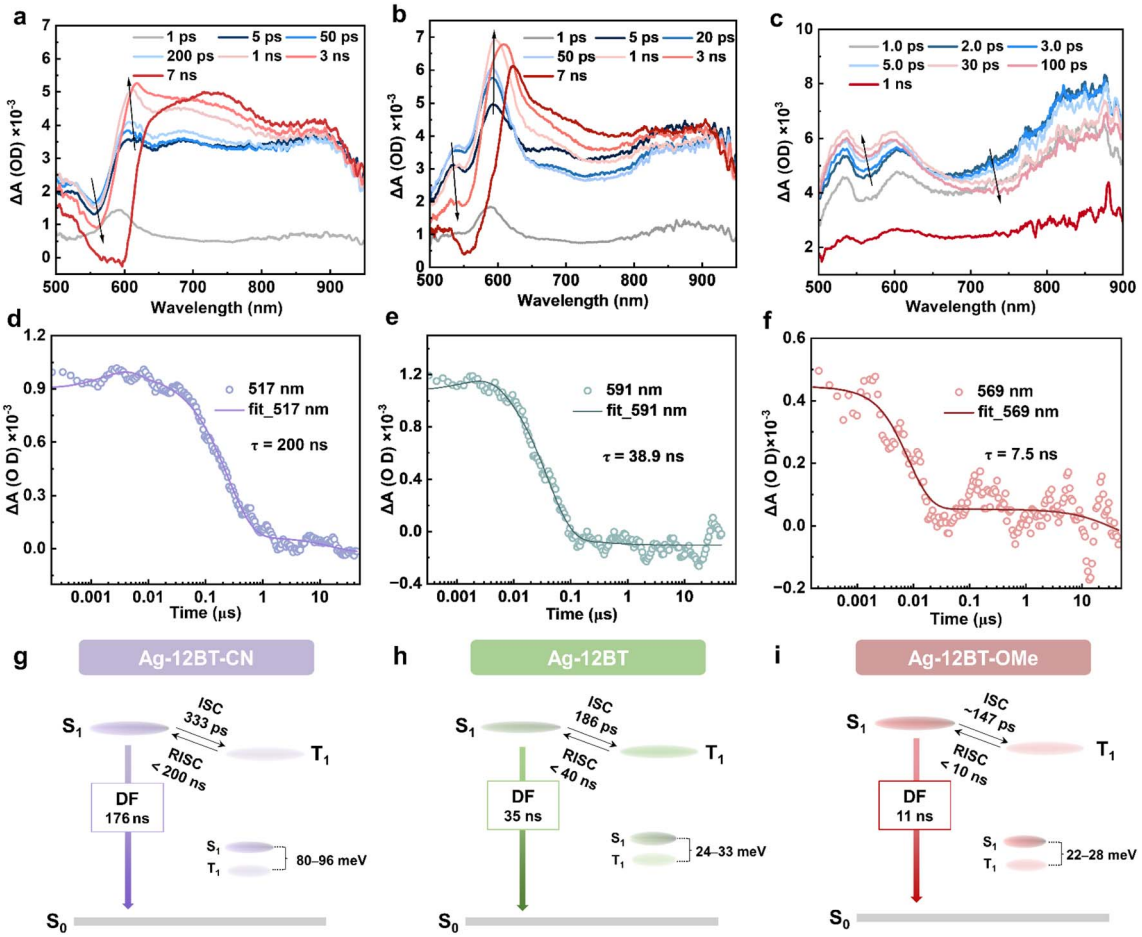

Fig. 4 Fs-TA spectra of (a) Ag-12BT-CN, (b) Ag-12BT, and (c) Ag-12BT-OMe in chlorobenzene solution (2 mg mL^{-1}), following excitation at 400 nm. The ns-transient kinetics of (d) Ag-12BT-CN at 819 nm, (e) Ag-12BT at 591 nm, and (f) Ag-12BT-OMe at 569 nm, following excitation at 400 nm. Schematic diagram of exciton dynamics of (g) Ag-12BT-CN, (h) Ag-12BT, and (i) Ag-12BT-OMe based on TA and transient PL experiments.

After that, the S_1 conformation reorganization occurred with time constants of 1.2–6.6 ps. For Ag-12BT-CN, in the time range of 5 ps–3 ns, the amplitude of the PIA signal at 500–600 nm gradually decreased, accompanied by its increase at 600–625 nm, with a time constant of 333 ps (Fig. 4a and S13a†), which could be attributed to the ISC process. This value is consistent with the previously reported ISC rates (tens to hundreds of ps) for CMA complexes in the literature.[38g–l,39,40] Comparatively, the ISC process of Ag-12BT occurred within 1 ns with a faster time constant of 186 ps (Fig. 4b and S13b†). For Ag-12BT-OMe, the PIA signals at 500–650 nm and 700–800 nm increased and dropped, respectively, within 30 ps, while all the signals dropped significantly after 30 ps. This may be caused by the PIA signal overlaps of singlet and triplet excited states. The ISC time constant of Ag-12BT-OMe was roughly determined as 147 ps according to the dynamic curves (Fig. S13c†). In the ns-scale time range, the amplitude of the PIA signals in all detecting wavelengths decreased significantly for all these complexes, indicating the decay of T_1 excitons (including reverse ISC and nonradiative processes) (Fig. 4d–f and S14†). Similar to the sequence of ISC rates, the lifetimes of T_1 excitons followed the trend of 200 ns (Ag-12BT-CN) > 38.9 ns (Ag-12BT) > 7.5 ns (Ag-12BT-OMe), well consistent with the emission lifetimes of these complexes recorded in transient PL in solutions (Fig. 3d and Table 1). Combined with the above PL studies, Fig. 4g–i depicts the simplified excited-state dynamics of these complexes. Basically, all the Ag(I) complexes experienced the fast ISC process with rate constants of 3.0–6.8 × 10^9 s^{-1}, followed by a fast reverse ISC (RISC) process and further singlet radiation. In particular, Ag-12BT and Ag-12BT-OMe underwent the ultrafast RISC process with the rate constants of *ca.* 10^8 s^{-1}, among one of the highest values for TADF emitters.

In view of the outstanding optical properties with high Φ_{PL} and short TADF lifetimes, solution-processed OLEDs were fabricated to explore the electroluminescence (EL) performance of these Ag(I) complexes. Before the device characterization, we used atomic force microscopy to study the film-forming ability of the Ag(I) emitters. The spin-coated doped films of the Ag(I) emitters afforded smooth surfaces with root-mean-square roughness values of ~0.3 nm (Fig. S15†), which are feasible for the fabrication of solution-processed OLEDs. The device structure consisted of indium tin oxide (ITO)/poly-(3,4-

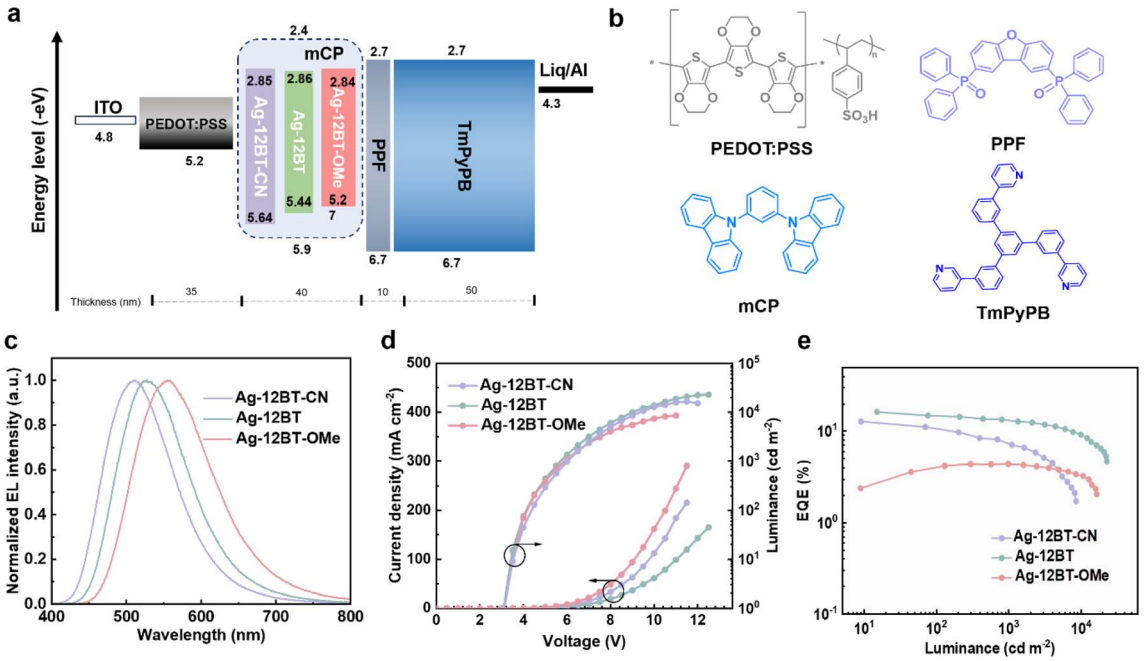

Fig. 5 (a) Device structure of the optimal devices based on Ag-12BT-CN, Ag-12BT, and Ag-12BT-OMe. (b) Molecular structures of the functional materials used in the devices. (c) Normalized EL spectra and (d) current density–voltage–luminance curves of the devices based on Ag-12BT-CN, Ag-12BT, and Ag-12BT-OMe. (e) External quantum efficiency as a function of luminance for the devices based on Ag-12BT-CN, Ag-12BT, and Ag-12BT-OMe.

Table 2 Summary of EL characteristics of the optimal devices

Emitter	V_{on}[a] [V]	CE[b] [cd A^{-1}]	PE[c] [lm W^{-1}]	EQE[d] [%]	EL_{peak} [nm]	CIE (x, y)
Ag-12BT-CN	3.2	35.0, 21.6, 19.0	31.4, 14.2, 10.0	12.8, 10.6, 7.1	512	0.26, 0.45
Ag-12BT	3.2	48.7, 44.3, 39.9	43.7, 34.8, 22.8	16.2, 14.8, 13.4	528	0.33, 0.53
Ag-12BT-OMe	3.2	12.8, 12.3, 12.7	6.5, 4.8, 3.3	4.4, 4.1, 4.3	558	0.41, 0.53

[a] The turn-on voltage recorded at a luminance of 1 cd m^{-2}. [b] Current efficiency. [c] Power efficiency. [d] External quantum efficiency at the maximum, 100 and 1000 cd m^{-2}.

ethylenedioxythiophene):poly(styrenesulfonate) (PEDOT:PSS) (35 nm)/emissive layer (40 nm)/dibenzo[b,d]furan-4,6-diylbis(-diphenylphosphine oxide) (PPF) (10 nm)/1,3,5-tri[(3-pyridyl)-phen-3-yl]benzene (TmPyPB) (50 nm)/8-hydroxyquinolinolato-lithium (Liq) (1 nm)/Al (100 nm) (Fig. 5a and b). The Ag(I)-CMA complexes were doped into the typical host mCP with an optimal 30 wt% concentration. As shown in Fig. 5c and Table 2, the devices based on Ag-12BT-CN, Ag-12BT, and Ag-12BT-OMe displayed green to yellow EL emissions peaking at 512, 528, and 558 nm, along with the corresponding CIE coordinates of (0.26, 0.45), (0.33, 0.53), and (0.41, 0.53), respectively. As illustrated in Fig. 5d, all the devices had low turn-on voltages of 3.2 V, implying the balanced charge carrier injection and transport in the devices. Due to the higher Φ_{PL} of Ag-12BT-CN and Ag-12BT, the resulting devices delivered higher EQEs of 12.8% and 16.2% at 10–15 cd m^{-2}, respectively, compared with 4.4% EQE of the Ag-12BT-OMe-based device (Table 2). To the best of our knowledge, the EQE of 16.2% represents the state-of-the-art EL efficiency for Ag(I) emitters (excluding Ag clusters containing Au and/or Pt atoms) (Table S5†).[35,36,46] Moreover, the Ag-12BT-based device afforded an alleviated efficiency roll-off value of 17.2% together with the high EQE of 13.4% at the practical luminance of 1000 cd m^{-2}. This roots from the short emission lifetimes and ultrafast spin-flip processes of the emitter, benefiting the triplet harvesting meanwhile preventing the triplet-involved annihilation at high current densities. Interestingly, the champion emitter Ag-12BT supported its devices exhibiting remarkably high EQEs of 12.2–16.2% with the doping concentrations in the range of 20–50 wt% (Fig. S16 and Table S6†), highlighting the suppressed concentration-caused emission quenching of Ag-12BT.

Conclusions

In summary, we have developed a series of two-coordinate Ag(I) complexes bearing the carbene-metal-amide (CMA) motif. By tuning the π-donating strength of the amide ligands, these complexes delivered tunable emission colors with a large radiative rate constant of ~10^7 s^{-1} as well as distinct thermally activated delayed fluorescence (TADF) properties with short

emission lifetimes of down to 11 ns in solution. The transient absorption spectroscopies disclosed that Ag-12BT and Ag-12BT-OMe in solution experience ultrafast spin-flip dynamics with large forward and reverse intersystem crossing (ISC) rate constants of up to $\sim 10^9$ s^{-1} and $\sim 10^8$ s^{-1}, respectively. Inspiringly, Ag-12BT exhibits the best emission performance in the thin film state, having the high Φ_{PL} of 72%, the short lifetime of 330 ns, and the fast radiative rate of 2.2×10^6 s^{-1}. The resultant solution-processed OLEDs based on these complexes achieved record external quantum efficiencies of up to 16.2%, representing the state-of-the-art efficiency performance for the OLEDs based on Ag(I) complexes. This work not only unlocks the large potential of Ag(I)-CMA complexes in developing high-efficiency OLEDs but also opens a new avenue for the design of short-lived TADF materials.

Data availability

The data supporting the findings of this study are available within the article and its ESI.†

Author contributions

A. Y. and N. L. contributed equally to this work. S. G. conceived and designed the project. A. Y. synthesized the complexes and measured photophysical properties. N. L. and C. Y. fabricated and characterized the devices. X. C. and J. X. performed transient absorption spectroscopy. A. Y. conducted the quantum chemical calculations. S. G. supervised this research. A. Y. and S. G. co-wrote the manuscript. All the authors discussed the results and contributed to the manuscript.

Conflicts of interest

S. G. and A. Y. are inventors on a patent application related to this work (CN patent application no. 202310604157.4) filed by Wuhan University. The authors declare no other competing interests.

Acknowledgements

S. G. gratefully acknowledges financial support from the National Natural Science Foundation of China (52022071). The numerical calculations in this paper were done on the supercomputing system in the Supercomputing Center of Wuhan University. The authors thank Prof. Cheng Zhong (Wuhan University) for the helpful suggestion on theoretical calculations. The authors thank the Core Facility of Wuhan University for atomic force microscopy measurements.

References

1 (*a*) C. Bizzarri, E. Spuling, D. M. Knoll, D. Volz and S. Brase, *Coord. Chem. Rev.*, 2018, **373**, 49–82; (*b*) H. Madec, F. Figueiredo, K. Cariou, S. Roland, M. Sollogoub and G. Gasser, *Chem. Sci.*, 2023, **14**, 409–442.
2 (*a*) Y. Liu, S.-C. Yiu, C.-L. Ho and W.-Y. Wong, *Coord. Chem. Rev.*, 2018, **375**, 514–557; (*b*) R.-Q. Xia, Z.-N. Liu, Y.-Y. Tang, X. Luo, R.-J. Wei, T. Wu, G.-H. Ning and D. Li, *Chem. Sci.*, 2024, **15**, 14513–14520.
3 X. Li, Y. Xie and Z. Li, *Chem.–Asian J.*, 2021, **16**, 2817–2829.
4 R. C. Evans, P. Douglas and C. J. Winscom, *Coord. Chem. Rev.*, 2006, **250**, 2093–2126.
5 Q. Zhao, F. Li and C. Huang, *Chem. Soc. Rev.*, 2010, **39**, 3007–3030.
6 A. Ramírez-Solís, V. Vallet, C. Teichteil, T. Leininger and J. P. Daudey, *J. Chem. Phys.*, 2001, **115**, 3201–3207.
7 (*a*) R. Hamze, J. L. Peltier, D. Sylvinson, M. Jung, J. Cardenas, R. Haiges, M. Soleilhavoup, R. Jazzar, P. I. Djurovich, G. Bertrand and M. E. Thompson, *Science*, 2019, **363**, 601–606; (*b*) K. A. Spence, J. V. Chari, M. Di Niro, R. B. Susick, N. Ukwitegetse, P. I. Djurovich, M. E. Thompson and N. K. Garg, *Chem. Sci.*, 2022, **13**, 5884–5892.
8 J. R. Kirchhoff, R. E. Gamache Jr, M. W. Blaskie, A. A. Del Paggio, R. K. Lengel and D. R. McMillin, *Inorg. Chem.*, 1983, **22**, 2380–2384.
9 J. C. Deaton, S. C. Switalski, D. Y. Kondakov, R. H. Young, T. D. Pawlik, D. J. Giesen, S. B. Harkins, A. J. M. Miller, S. F. Mickenberg and J. C. Peters, *J. Am. Chem. Soc.*, 2010, **132**, 9499–9508.
10 A. Tsuboyama, K. Kuge, M. Furugori, S. Okada, M. Hoshino and K. Ueno, *Inorg. Chem.*, 2007, **46**, 1992–2001.
11 M. Hashimoto, S. Igawa, M. Yashima, I. Kawata, M. Hoshino and M. Osawa, *J. Am. Chem. Soc.*, 2011, **133**, 10348–10351.
12 A. Schinabeck, J. Chen, L. Kang, T. Teng, H. H. H. Homeier, A. F. Suleymanova, M. Z. Shafikov, R. Yu, C.-Z. Lu and H. Yersin, *Chem. Mater.*, 2019, **31**, 4392–4404.
13 R. Czerwieniec, M. J. Leitl, H. H. H. Homeier and H. Yersin, *Coord. Chem. Rev.*, 2016, **325**, 2–28.
14 C. E. Housecroft and E. C. Constable, *J. Mater. Chem. C*, 2022, **10**, 4456–4482.
15 N. Aizawa, Y. Harabuchi, S. Maeda and Y.-J. Pu, *Nat. Commun.*, 2020, **11**, 3909.
16 K. Matsumoto, T. Shindo, N. Mukasa, T. Tsukuda and T. Tsubomura, *Inorg. Chem.*, 2010, **49**, 805–814.
17 M. Osawa, I. Kawata, R. Ishii, S. Igawa, M. Hashimoto and M. Hoshino, *J. Mater. Chem. C*, 2013, **1**, 4375.
18 J. Chen, T. Teng, L. Kang, X.-L. Chen, X.-Y. Wu, R. Yu and C.-Z. Lu, *Inorg. Chem.*, 2016, **55**, 9528–9536.
19 M. Z. Shafikov, A. F. Suleymanova, R. Czerwieniec and H. Yersin, *Chem. Mater.*, 2017, **29**, 1708–1715.
20 X.-M. Gan, R. Yu, X.-L. Chen, M. Yang, L. Lin, X.-Y. Wu and C.-Z. Lu, *Dalton Trans.*, 2018, **47**, 5956–5960.
21 M. Z. Shafikov, A. F. Suleymanova, A. Schinabeck and H. Yersin, *J. Phys. Chem. Lett.*, 2018, **9**, 702–709.
22 A. V. Artem'ev, M. Z. Shafikov, A. Schinabeck, O. V. Antonova, A. S. Berezin, I. Y. Bagryanskaya, P. E. Plusnin and H. Yersin, *Inorg. Chem. Front.*, 2019, **6**, 3168–3176.
23 M. Klein, N. Rau, M. Wende, J. Sundermeyer, G. Chengz, C.-M. Che, A. Schinabeck and H. Yersin, *Chem. Mater.*, 2020, **32**, 10365–10382.
24 H. Yersin, R. Czerwieniec, M. Z. Shafikov and A. F. Suleymanova, *ChemPhysChem*, 2017, **18**, 3508–3535.

25 M. Z. Shafikov, R. Czerwieniec and H. Yersin, *Dalton Trans.*, 2019, **48**, 2802–2806.
26 C.-W. Hsu, C.-C. Lin, M.-W. Chung, Y. Chi, G.-H. Lee, P.-T. Chou, C.-H. Chang and P.-Y. Chen, *J. Am. Chem. Soc.*, 2011, **133**, 12085–12099.
27 F. So, C. Adachi, H. Yersin, M. J. Leitl and R. Czerwieniec, in *Organic Light Emitting Materials and Devices XVIII*, 2014, vol. 9183, pp. 43–53.
28 M. Osawa, M. Hashimoto, I. Kawata and M. Hoshino, *Dalton Trans.*, 2017, **46**, 12446–12455.
29 M. Z. Shafikov, A. F. Suleymanova, R. Czerwieniec and H. Yersin, *Inorg. Chem.*, 2017, **56**, 13274–13285.
30 J.-H. Jia, D. Liang, R. Yu, X.-L. Chen, L. Meng, J.-F. Chang, J.-Z. Liao, M. Yang, X.-N. Li and C.-Z. Lu, *Chem. Mater.*, 2019, **32**, 620–629.
31 M. Y. Wong and E. Zysman-Colman, *Adv. Mater.*, 2017, **29**, 1605444.
32 Z. Yang, Z. Mao, Z. Xie, Y. Zhang, S. Liu, J. Zhao, J. Xu, Z. Chi and M. P. Aldred, *Chem. Soc. Rev.*, 2017, **46**, 915–1016.
33 J. Jayabharathi, V. Thanikachalam and S. Thilagavathy, *Coord. Chem. Rev.*, 2023, **483**, 215100.
34 H.-T. Mao, G.-F. Li, G.-G. Shan, X.-L. Wang and Z.-M. Su, *Coord. Chem. Rev.*, 2020, **413**, 213283.
35 A. S. Romanov, S. T. E. Jones, L. Yang, P. J. Conaghan, D. Di, M. Linnolahti, D. Credgington and M. Bochmann, *Adv. Opt. Mater.*, 2018, **6**, 1801347.
36 T. Teng, K. Li, G. Cheng, Y. Wang, J. Wang, J. Li, C. Zhou, H. Liu, T. Zou, J. Xiong, C. Wu, H.-X. Zhang, C.-M. Che and C. Yang, *Inorg. Chem.*, 2020, **59**, 12122–12131.
37 W. Brütting, J. Frischeisen, T. D. Schmidt, B. J. Scholz and C. Mayr, *Phys. Status Solidi A*, 2013, **210**, 44–65.
38 (*a*) D. Di, A. S. Romanov, L. Yang, J. M. Richter, J. P. H. Rivett, S. Jones, T. H. Thomas, M. Abdi Jalebi, R. H. Friend, M. Linnolahti, M. Bochmann and D. Credgington, *Science*, 2017, **356**, 159–163; (*b*) S. Shi, M. C. Jung, C. Coburn, A. Tadle, D. Sylvinson, M. R, P. I. Djurovich, S. R. Forrest and M. E. Thompson, *J. Am. Chem. Soc.*, 2019, **141**, 3576–3588; (*c*) J. Li, L. Wang, Z. Zhao, X. Li, X. Yu, P. Huo, Q. Jin, Z. Liu, Z. Bian and C. Huang, *Angew. Chem., Int. Ed.*, 2020, **59**, 8210–8217; (*d*) A. S. Romanov, S. T. E. Jones, Q. Gu, P. J. Conaghan, B. H. Drummond, J. Feng, F. Chotard, L. Buizza, M. Foley, M. Linnolahti, D. Credgington and M. Bochmann, *Chem. Sci.*, 2020, **11**, 435–446; (*e*) T.-Y. Li, J. Schaab, P. I. Djurovich and M. E. Thompson, *J. Mater. Chem. C*, 2022, **10**, 4674; (*f*) C. N. Muniz, J. Schaab, A. Razgoniaev, P. I. Djurovich and M. E. Thompson, *J. Am. Chem. Soc.*, 2022, **144**, 17916–17928; (*g*) M. Gernert, L. Balles-Wolf, F. Kerner, U. Müller, A. Schmiedel, M. Holzapfel, C. M. Marian, J. Pflaum, C. Lambert and A. Steffen, *J. Am. Chem. Soc.*, 2020, **142**, 8897–8909; (*h*) R. Tang, S. Xu, T.-L. Lam, G. Cheng, L. Du, Q. Wan, J. Yang, F.-F. Hung, K.-H. Low, D. L. Phillips and C.-M. Che, *Angew. Chem., Int. Ed.*, 2022, **61**, e202203982; (*i*) H.-J. Wang, Y. Liu, B. Yu, S.-Q. Song, Y.-X. Zheng, K. Liu, P. Chen, H. Wang, J. Jiang and T.-Y. Li, *Angew. Chem., Int. Ed.*, 2023, **62**, e202217195; (*j*) Q. Gu, F. Chotard, J. Eng, A. P. M. Reponen, I. J. Vitorica-Yrezabal, A. W. Woodward, T. J. Penfold, D. Credgington, M. Bochmann and A. S. Romanov, *Chem. Mater.*, 2022, **34**, 7526–7542; (*k*) A. Ying, Y. Ai, C. Yang and S. Gong, *Angew. Chem., Int. Ed.*, 2022, **61**, e202210490; (*l*) R. Hamze, S. Shi, S. C. Kapper, D. S. Muthiah Ravinson, L. Estergreen, M. C. Jung, A. C. Tadle, R. Haiges, P. I. Djurovich, J. L. Peltier, R. Jazzar, G. Bertrand, S. E. Bradforth and M. E. Thompson, *J. Am. Chem. Soc.*, 2019, **141**, 8616–8626; (*m*) A. Ying, L. Zhan, Y. Tan, X. Cao, C. Yang and S. Gong, *Sci. China: Chem.*, 2023, **66**, 2274–2282; (*n*) J. Feng, A.-P. M. Reponen, A. S. Romanov, M. Linnolahti, M. Bochmann, N. C. Greenham, T. Penfold and D. Credgington, *Adv. Funct. Mater.*, 2021, **31**, 2005438.
39 (*a*) A. Ying and S. Gong, *Chem.–Eur. J.*, 2023, **29**, e2023018; (*b*) T.-Y. Li, S.-J. Zheng, P. I. Djurovich and M. E. Thompson, *Chem. Rev.*, 2024, **124**, 4332–4392; (*c*) Y. Tan, A. Ying, J. Xie, G. Xie and S. Gong, *Chem. Sci.*, 2024, **15**, 11382–11390.
40 D. S. M. Ravinson and M. E. Thompson, *Mater. Horiz.*, 2020, **7**, 1210–1217.
41 A. Ying, Y. Tan and S. Gong, *Adv. Opt. Mater.*, 2024, **12**, 2303333.
42 A. Ying, *CCDC Experimental Crystal Structure Determination*, 2024, p. 2305500, DOI: **10.5517/ccdc.csd.cc2hd1zy**.
43 A. V. Bondi, *J. Phys. Chem.*, 1964, **68**, 441–451.
44 (*a*) R. F. Bader, *Acc. Chem. Res.*, 1985, **18**, 9–15; (*b*) D. J. Pascoe, K. B. Ling and S. L. Cockroft, *J. Am. Chem. Soc.*, 2017, **139**, 15160–15167; (*c*) M. Liu, X. Han, H. Chen, Q. Peng and H. Huang, *Nat. Commun.*, 2023, **14**, 2500.
45 R. C. Hilborn, *Am. J. Phys.*, 1982, **50**, 982–986.
46 Z. Jiao, M. Yang, J.-Y. Wang, Y.-Z. Huang, P. Xie and Z.-N. Chen, *J. Mater. Chem. C*, 2021, **9**, 5528–5534.